Oscillating path between self-similarities in liquid pinch-off

Antoine Lagarde[a], Christophe Josserand[b], and Suzie Protière[a,1]

[a]Institut Jean Le Rond ∂'Alembert, Sorbonne Université, Centre National de la Recherche Scientifique, UMR 7190, F-75005 Paris, France; and [b]LadHyX, CNRS, Ecole Polytechnique, UMR 7646, 91128 Palaiseau, France

Edited by Michael Marder, University of Texas, Austin, TX, and accepted by Editorial Board Member John D. Weeks October 24, 2018 (received for review August 17, 2018)

Many differential equations involved in natural sciences show singular behaviors; i.e., quantities in the model diverge as the solution goes to zero. Nonetheless, the evolution of the singularity can be captured with self-similar solutions, several of which may exist for a given system. How to characterize the transition from one self-similar regime to another remains an open question. By studying the classic example of the pinch-off of a viscous liquid thread, we show experimentally that the geometry of the system and external perturbations play an essential role in the transition from a symmetric to an asymmetric solution. Moreover, this transient regime undergoes unexpected log-scale oscillations that delay dramatically the onset of the final self-similar solution. This result sheds light on the strong impact external constraints can have on predictions established to explain the formation of satellite droplets or on the rheological tests applied on a fluid, for example.

pinch-off | viscous | self-similarity | log-oscillation | external constraints

From the greedy child who wants to detach the last drop of tomato sauce from its container to his loving parents who desperately try to fix the dripping faucet (1), drop formation surrounds us in our daily life. It also concerns various applications, from the usual inkjet printing to transistor circuits (2) or even bioprinting of mammalian cells (3), for instance. Drop detachment corresponds to a liquid breakup that is obtained by the pinch-off of the final thin liquid thread. This pinch-off is mathematically described by a finite-time singularity, the minimal radius of the liquid thread $r_{\min}(z,t)$ being exactly zero for $t = t_{\rm po}$ and at $z = z_{\rm po}$. The mathematical analysis close to this singularity suggests different self-similar regimes, depending on the specific balance between inertia and viscous and capillary forces (4, 5). These different self-similar solutions have been observed experimentally in dedicated experiments (6, 7) as well as numerically (8, 9). However, recent experimental and numerical works have shown that the general situation is more complex (10–14): Transient dynamics and multiple transitions have been observed for the neck evolution, delaying the onset of self-similar regimes. During these transient dynamics, the minimum thread radius can follow the scalings of the different self-similar regimes. Thus, the link between the neck evolution and the liquid thread profile has to be questioned with respect to the self-similar solutions. Indeed, in practical situations, this result may have crucial implications for droplet release and rheological characterization. In this article, we propose an experiment to characterize and control this transient regime. We define the key parameters impacting the evolution of the neck during droplet breakup and we discriminate the different self-similar regimes.

We first place a circular aluminum cylinder at an oil–water interface. The cylinder is pinned at this interface and pulled downward with a stepper motor. We can thus control both the radius of the cylinder $R_{\rm cyl}$ and its vertical velocity $v_{\rm cyl}$ (Fig. 1*B*). To move the cylinder quasi-statically ($v_{\rm cyl} = 0$), we control its vertical motion in 10-μm increments close to pinch-off and wait a few seconds between each step (*Materials and Methods*). A stretched meniscus is formed between this moving cylinder and the layer of oil. The oil thread thins until it finally breaks up (Fig. 1*D* and Movie S2). We measure the evolution of the neck during this process. This experiment enables us to investigate the impact of a vertical velocity on the evolution of the detachment of an oil drop in a liquid bath. We then compare this situation to a rising oil droplet detaching from a circular nozzle immersed in water, for different needle radii $R_{\rm needle}$ (Fig. 1*A*).

The vertical velocity of the cylinder in Fig. 1*D* imposes boundary conditions dramatically different from those of the rising droplet in Fig. 1*C* (Movies S1 and S2). Qualitatively, it is already clear that the shapes of the liquid threads are different between the two situations: In particular, the symmetry of the viscous filament at the detachment of the droplet is not recovered when the interface is pulled downward.

The characteristic lengthscale l_μ and timescale t_μ of such viscous dynamics can be defined by

$$l_\mu = \frac{\mu^2}{\gamma\rho} \qquad t_\mu = \frac{\mu^3}{\gamma^2\rho} \qquad [1]$$

with μ and ρ the dynamic viscosity and density of the oil, and γ the oil–water interfacial tension. We describe the dynamics of pinch-off through the Ohnesorge number based on the oil properties:

$$Oh = \frac{\mu}{\sqrt{\rho\gamma R}}. \qquad [2]$$

Significance

Droplet pinch-off is one of the most commonly examined free surface flows displaying a finite-time singularity and can serve as the basis upon which to better understand similar singular behavior. A liquid filament connecting the droplet to the rest of the fluid thins before it breaks and passes through several self-similar regimes that have been thought independent of external conditions. These regimes are essentially asymptotic, and it is an open question how exactly the system passes through them. We find to our surprise that external conditions strongly affect the transient path connecting these regimes and even can temporarily prevent the fluid thread from evolving through self-similar profiles. Our results raise many questions about the influence of boundary conditions on such self-similar dynamics.

Author contributions: A.L. and S.P. designed research; A.L. performed research; A.L., C.J., and S.P. analyzed data; and A.L., C.J., and S.P. wrote the paper.

The authors declare no conflict of interest.

This article is a PNAS Direct Submission. M.M. is a guest editor invited by the Editorial Board.

[1]To whom correspondence should be addressed. Email: protiere@ida.upmc.fr.

This article contains supporting information online at www.pnas.org/lookup/suppl/doi:10.1073/pnas.1814242115/-/DCSupplemental.

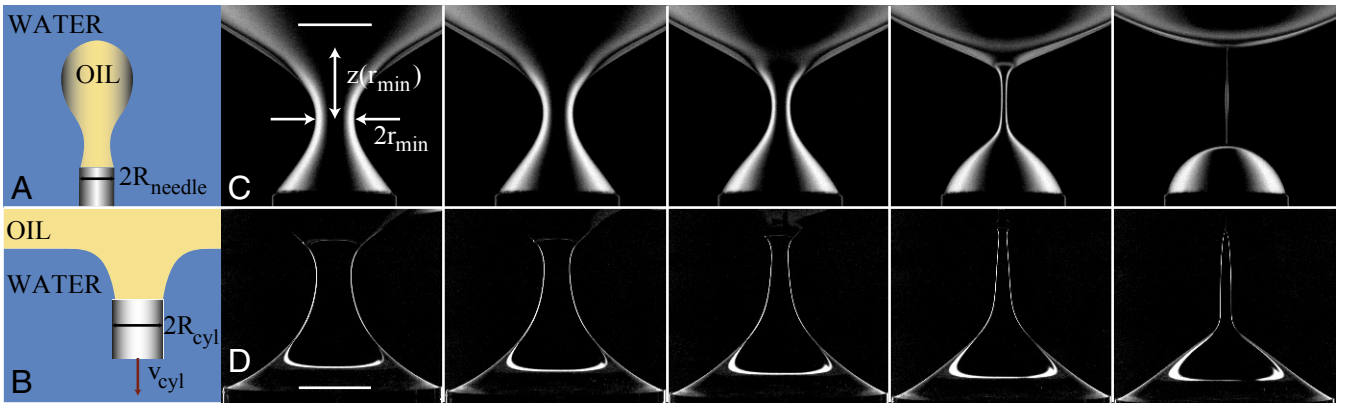

Fig. 1. Experimental setups and visualizations of the thinning of a viscous filament in various configurations. (*A*) Schematic of the first experimental configuration. An oil droplet is formed via a needle of radius R_{needle} at a low flow rate inside a bath of water. (*B*) Second experimental configuration. An oil–water interface is pulled downward with an aluminum cylinder of radius R_{cyl} at a given velocity v_{cyl}, until the oil meniscus formed during the process breaks. (*C*) Time lapse of the detachment of an oil droplet from a nozzle ($2R_{needle}$ = 1.65 mm). Time between two images: 2.5 ms. [Scale bar: 1 mm (Movie S1).] (*D*) Time lapse showing the thinning of an oil filament formed by pulling an oil–water interface with a cylinder of radius $2R_{cyl}$ = 30 mm at a vertical velocity of v_{cyl} = 30 mm·s^{-1}. Time between two images: 25 ms. (Scale bar: 10 mm.) In both sequences, the final image corresponds to the exact moment of pinch-off (Movie S2).

Here, R stands for the initial radius of the system (either R_{cyl} or R_{needle}, depending on the experiment). In this study, we limited ourselves to Ohnesorge numbers between 0.1 and 0.7, corresponding to R varying between 0.5 and 15 mm.

We measure the time evolution of r_{min} and $z(r_{min})$ (notations in Fig. 1*C*). The thinning dynamics begin by the destabilization of a fluid cylinder due to the Plateau–Rayleigh instability (15, 16). Once the perturbation of the ideal liquid cylinder is large enough, the linear stability approach can no longer hold. Thinning is then governed by a nonlinear competition between surface tension and viscosity (17), where the minimum radius r_{min} and its vertical position z(r_{min}) evolve according to Eq. **3** (viscous regime),

$$\frac{r_{min}}{l_\mu} = 0.0709\,\frac{(\tau - t_0)}{t_\mu} \qquad \frac{z(r_{min})}{l_\mu} \sim \left(\frac{\tau}{t_\mu}\right)^{\beta}, \qquad [3]$$

with $\tau = t_{po} - t$ the remaining time before breakup and β = 0.175. t_0 accounts for the fact that this approach is not valid all of the way to the pinch-off. Indeed, the velocity of the fluid increases until inertia can no longer be neglected. At some point, a balance between surface tension, viscosity, and inertia (18) is needed and leads to Eq. **4** (inertial–viscous regime):

$$\frac{r_{min}}{l_\mu} = 0.0304\,\frac{\tau}{t_\mu} \qquad \frac{z(r_{min})}{l_\mu} \sim \left(\frac{\tau}{t_\mu}\right)^{0.5}. \qquad [4]$$

To facilitate further references to the two previous linear evolutions of r_{min}, we designate by u_v and u_{iv} the slopes of these two regimes, as defined in the following equation:

$$u_v = 0.0709\frac{\gamma}{\mu} \qquad u_{iv} = 0.0304\frac{\gamma}{\mu}. \qquad [5]$$

These solutions are universal: Whatever boundary and initial conditions are restricting the system, at a given time a viscous system will transit from the viscous regime to the inertial–viscous one. Various experiments have confirmed these scalings (19) and described the shape of the viscous thread for both regimes (20): symmetric for the viscous regime and asymmetric for the inertial–viscous one. When the viscosity of the surrounding fluid is taken into account, theory predicts the existence of a last regime (21), where both r_{min} and $z(r_{min})$ evolve linearly with τ.

In Fig. 2, we compare the evolution of the minimum radius r_{min} of a liquid neck in the classic case of an oil drop detaching from a needle (green circles) and a cylinder pulled from an oil–water interface (black stars), as a function of time before breakup τ. The curves should be read from right to left, with a monotonic decrease of r_{min} as τ gets closer to zero. In the first situation, we recover precisely the different regimes described previously: first an exponential decrease of r_{min} reminiscent of the Plateau–Rayleigh linear instability, followed by two nonlinear successive regimes where r_{min} decreases linearly, adequately fitted by the

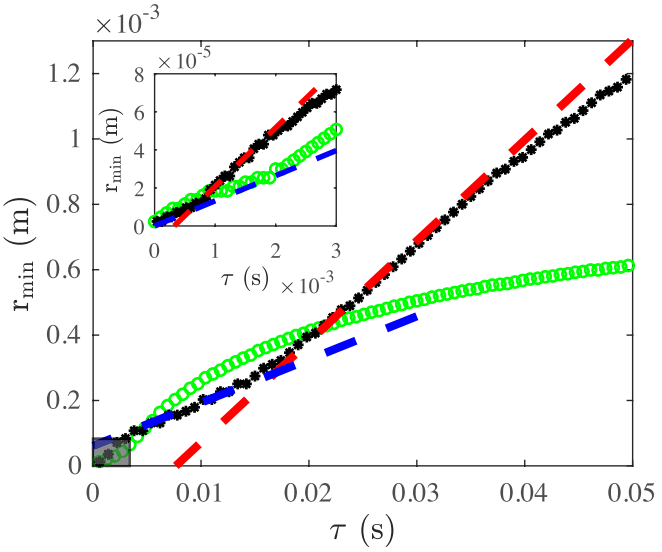

Fig. 2. Experimental evidence of a variation in the transient regime for different external constraints during the breakup of an oil filament in water. Shown is variation of the minimum neck radius with time until breakup for the thinning of a stretched oil meniscus inside water (black stars: $2R_{cyl}$ = 20 mm, v_{cyl} = 1 mm·s^{-1}) and for the pinch-off of an oil droplet from a nozzle (green circles: $2R_{needle}$ = 1.65 mm). The dashed lines represent the self-similar linear evolution describing, respectively, the viscous (red dashed line, Eq. **3**) and inertial–viscous regimes (blue dashed line, Eq. **4**). (*Inset*) Zoom-in of the evolution of r_{min} in the final moments before pinch-off ($\tau < 3$ ms), as a function of time before breakup. The error bars are negligible (smaller than the size of an individual symbol) and thus are not displayed for clarity.

theoretical predictions of Eqs. **3** (slope u_v) and **4** (slope u_{iv}). In the second situation, when the cylinder is pulling the interface, we also observe in the final stages of the pinching the same two linear decays, with slopes comparable to u_{iv} and u_v (Fig. 2, *Inset*). But interestingly, for $\tau > 3$ ms, the dynamics differ drastically. Instead of the classic exponential decay, we observe a succession of linear evolutions, with slopes similar to u_{iv} (5 ms $< \tau <$ 15 ms) or u_v (15 ms $< \tau <$ 35 ms). For longer times, we recover the exponential decrease of the minimum radius, characteristic of the Plateau–Rayleigh instability.

We do recover the theoretical slopes predicted by Eqs. **3** and **4** (Fig. 2), but in the configuration of a stretched meniscus, we moreover observe oscillations from one slope to another. Several differences between the two experiments described here can be highlighted to account for these distinct behaviors: the larger diameter of the cylinder compared with the needle (approximately 10 times larger), its vertical velocity since only buoyancy helps the oil drop to rise whereas the cylinder pulls the interface downward at velocity $v_{\mathrm{cyl}} = 1$ mm·s^{-1}, and finally the direction of motion of the oil droplet (downward for the cylinder and upward for the needle).

To identify the different regimes correctly, we plot $\dot{r}_{\mathrm{min}}$, the slope of r_{min} as a function of τ (14). Using this representation, each linear evolution of r_{min} now appears as a constant (u_v for the viscous regime and u_{iv} for the inertial–viscous one). Moreover, the curves are plotted in log-scale $\dot{r}_{\mathrm{min}}$ as a function of r_{min} instead of τ, since the measurement of r_{min} is more simple than the exact determination of the breakup point, making comparisons between experiments easier. Fig. 3 displays such measurements for three different configurations: the oil drop released from a nozzle in surrounding water ($2R_{\mathrm{needle}} = 1.65$ mm), the quasi-static pulldown of a cylinder from the same interface with a diameter comparable to the diameter of the nozzle ($2R_{\mathrm{cyl}} = 2$ mm), and finally the pulldown of a large cylinder ($2R_{\mathrm{cyl}} = 20$ mm) at a constant velocity $v_{\mathrm{cyl}} = 1$ mm/s.

The results for the configurations where a drop detaches from a needle (green circles) and an interface is pulled down quasi-statically with a cylinder of the same diameter (red triangles) are identical: an exponential increase of $\dot{r}_{\mathrm{min}}$, followed by a first plateau at $\dot{r}_{\mathrm{min}} \approx u_v$, and a final regime at $\dot{r}_{\mathrm{min}} \approx u_{iv}$ (Fig. 3). As the two curves are similar, we can exclude the direction of motion as a possible explanation for the different evolution of r_{min} in the two different experiments: As expected, gravity does not play a role in the self-similar regimes observed at short timescales. The black curve is, however, drastically different: $\dot{r}_{\mathrm{min}}$ presents a quasi-sinusoidal oscillation in log-scale, and only the last stages of the dynamics appear comparable between all experiments. As intuited with Fig. 2, we observe an oscillation between the two self-similar regimes. This result also emphasizes the existence of a given period of oscillation in the $\log(r_{\mathrm{min}})$ variable.

Unlike the experiment where a drop detaches from a nozzle, when pulling the oil–water interface downward with a cylinder, we can strongly vary independently the parameters at play, R_{cyl} and v_{cyl}, as shown in Fig. 4. We observe a log-oscillation of $\dot{r}_{\mathrm{min}}$ when R_{cyl} or v_{cyl} increases. When the detachment is quasi-static, i.e., $v_{\mathrm{cyl}} = 0$ (orange circles in Fig. 4), the oscillation appears and grows when $2R_{\mathrm{cyl}} > 8$ mm. When $R_{\mathrm{cyl}} = 5$ mm, $\dot{r}_{\mathrm{min}}$ oscillates only for the highest pulling velocity ($v_{\mathrm{cyl}} = 30$ mm/s). Finally, when $R_{\mathrm{cyl}} = 8$ mm, oscillations are always present. For the smallest cylinder $R_{\mathrm{cyl}} = 2$ mm, we do not observe oscillations using our experimental setup. This result confirms the numerical observations of ref. 14 where they find a similar oscillatory convergence in log-scale toward a self-similar regime. We show that external conditions (size and vertical velocity of the cylinder) play an essential role in the triggering of the oscillation in log-scale.

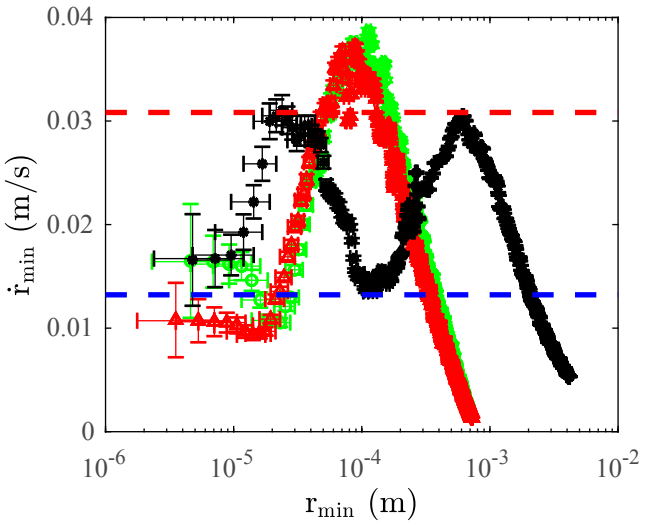

Fig. 3. Presence of an oscillation between linear evolutions when a large cylinder pulls down an oil–water interface. Shown is the time derivative of the minimum radius $\dot{r}_{\mathrm{min}}$ as a function of r_{min}, for three typical experiments. Green circles: oil droplet rising in water and finally detaching from a needle ($2R_{\mathrm{needle}} = 1.65$ mm). Red triangles: interface pulled quasi-statically by a cylinder ($2R_{\mathrm{cyl}} = 2$ mm, $v_{\mathrm{cyl}} = 0$ mm·s^{-1}). Black stars: oil–water interface pulled down by a larger cylinder ($2R_{\mathrm{cyl}} = 20$ mm, $v_{\mathrm{cyl}} = 1$ mm·s^{-1}). The dashed lines represent the theoretical linear self-similar regimes describing the viscous regime (red dashed line, $\dot{r}_{\mathrm{min}} = u_v$) and the inertial–viscous regime (blue dashed line, $\dot{r}_{\mathrm{min}} = u_{iv}$).

For every experiment, we can also measure the frequency of oscillation in log-scale ω_i and study its dependence with the different parameters [using the fit $\dot{r}_{\mathrm{min}} = A + B\sin(\omega_i \log t + C)\exp(D \log t)$]. For the range of parameters we have explored, ω_i is constant and does not depend on the various parameters of the different experiments we have investigated (*SI Appendix*, Fig. S1). This is consistent with the natural time dependence arising when a perturbation analysis is performed around the self-similar dynamics (*Materials and Methods*). The log-scale oscillation frequency depends only on the dynamical system and not on the external conditions.

Finally, we check whether the profiles are self-similar in the linear transient regimes observed during these oscillations. To that end, we report the profiles of the liquid thread and define rescaled variables according to Eqs. **3** and **4**,

$$\xi_1 = \frac{(z - z(r_{\mathrm{min}}))}{l_\mu^{0.5} r_{\mathrm{min}}^{0.5}}, \qquad H(\xi_1) = \frac{r}{r_{\mathrm{min}}} \qquad \textbf{[6]}$$

$$\xi_2 = \frac{(z - z(r_{\mathrm{min}}))}{l_\mu^{0.825} r_{\mathrm{min}}^{0.175}}, \qquad H(\xi_2) = \frac{r}{r_{\mathrm{min}}}. \qquad \textbf{[7]}$$

Since r_{min} decreases linearly with time (in each linear regime), we use r_{min} instead of τ to rescale both axes. As a consequence, the minimum radius of the thread is located at $\xi = 0$ and $H = 1$. ξ_1 and ξ_2 are made dimensionless using the characteristic length-scale l_μ. The profiles are relatively flat around r_{min}, which can make the determination of z(r_{min}) difficult. We thus shift the profiles in the ξ direction to superimpose the rescaled profiles (7). When $\dot{r}_{\mathrm{min}} = u_v$ (resp. $\dot{r}_{\mathrm{min}} = u_{iv}$), the profiles can be rescaled using Eq. **7** (resp. Eq. **6**).

Fig. 5 shows the rescaled profiles for two cylinder diameters pulling down the interface, during each of the linear regions ($\dot{r}_{\mathrm{min}}$ constant). In *A* and *B*, $R_{\mathrm{cyl}} = 2$ mm and no log-oscillation is observed: The profiles are rather well superimposed in each

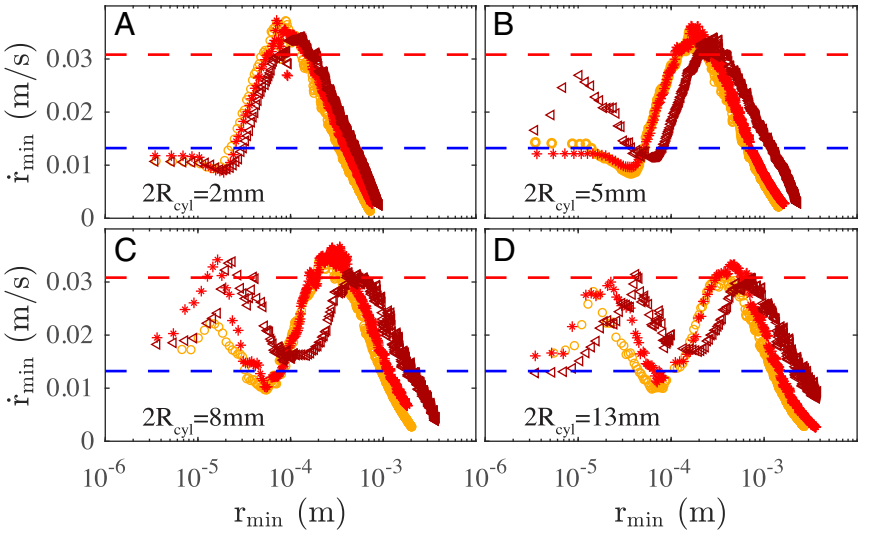

Fig. 4. Role of external conditions on the evolution of the thinning of a liquid thread pulled from an oil–water interface. We observe a log-oscillation of $\dot{r}_{\min}$ when $R_{\rm cyl}$ and $v_{\rm cyl}$ increase. We plot the time derivative $\dot{r}_{\min}$ as a function of $r_{\min}$, the minimum radius, for different cylinder diameters [(*A*) $2R_{\rm cyl}$ = 2 mm, (*B*) $2R_{\rm cyl}$ = 5 mm, (*C*) $2R_{\rm cyl}$ = 8 mm, and (*D*) $2R_{\rm cyl}$ = 13 mm] and different pulling velocities (orange circles, $v_{\rm cyl}$ = 0 mm/s; red crosses, $v_{\rm cyl}$ = 1 mm/s; dark-red triangles, $v_{\rm cyl}$ = 30 mm/s). The dashed lines represent the theoretical linear evolutions describing the self-similar viscous (red dashed line, $\dot{r}_{\min} = u_v$) and inertial–viscous (blue dashed line, $\dot{r}_{\min} = u_{iv}$) regimes, respectively.

of these regions, and we also recover the symmetry of the viscous regime around $r_{\min}$ (Fig. 5*B*). Moreover, the collapse of the self-similar curves is valid only around the position of the minimum radius.

Fig. 5 *C*–*F* shows the rescalings for $R_{\rm cyl}$ = 13 mm, when $\dot{r}_{\min}$ oscillates. The rescaling is also rather good close to the pinch-off (Fig. 5*C*), and the three profiles are well superimposed. We thus recover the final inertial–viscous regime, just like in the

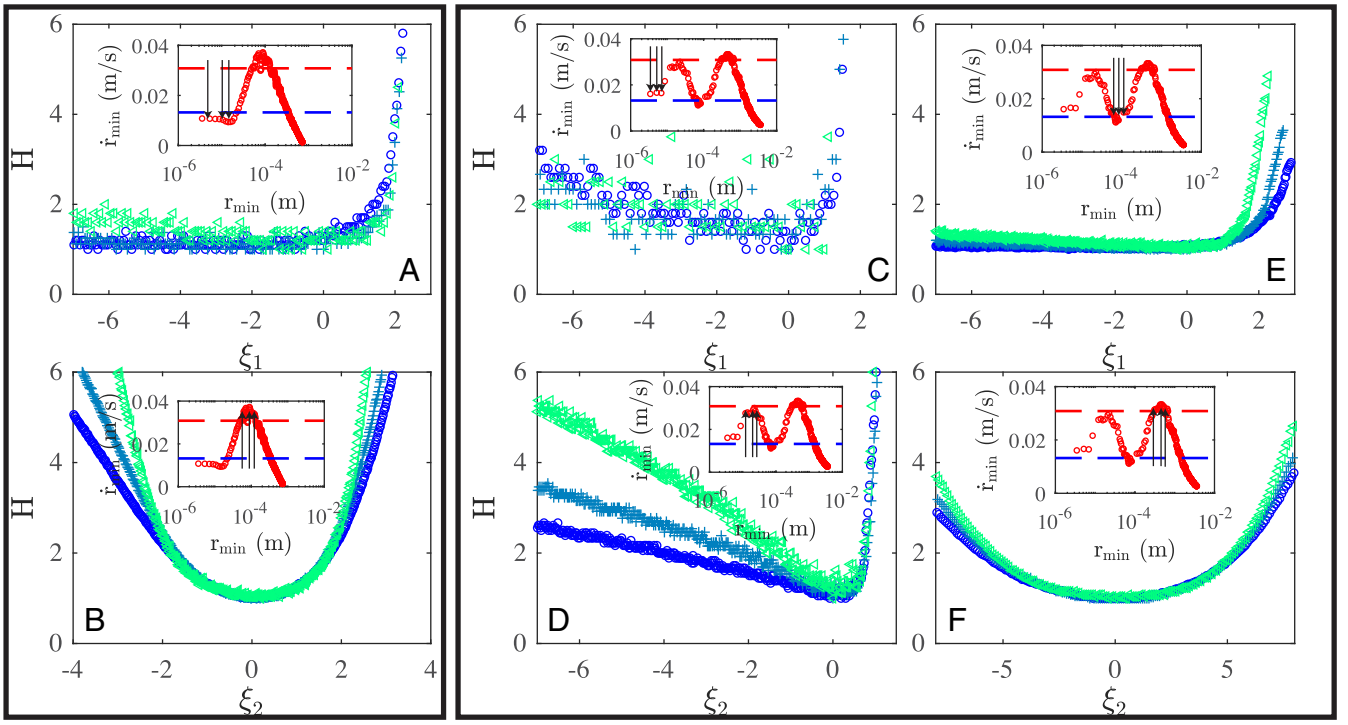

Fig. 5. Comparison of the rescaled profiles of the experimental data, obtained from an oil meniscus formed between cylinders of two different sizes when pulling down an oil–water interface. *Insets* show $\dot{r}_{\min}$ as a function of $r_{\min}$ in each case, with arrows indicating the profiles chosen in the main plot. Here again, the dashed lines represent the theoretical linear self-similar regimes describing, respectively, the viscous regime (red dashed line, $\dot{r}_{\min} = u_v$) and the inertial–viscous regime (blue dashed line, $\dot{r}_{\min} = u_{iv}$). The rescaled profiles represent H as a function of ξ_1 if the expected regime is inertial–viscous or ξ_2 if it is expected to be only viscous (Eqs. **6** and **7**). *A* and *B* show $2R_{\rm cyl}$ = 2 mm, $v_{\rm cyl}$ = 0 mm·s^{-1}. *C*–*F* show $2R_{\rm cyl}$ = 13 mm, $v_{\rm cyl}$ = 1 mm·s^{-1}. The profiles identified by black arrows in each *Inset* are represented from left to right by green triangles, light-blue crosses, and dark-blue circles. No error bars are displayed so that the distinction between the different curves remains possible.

classic case of an oil droplet detaching from a needle. Similarly, after the exponential regime, the system is well described by the viscous regime (Fig. 5*F*), with the expected value of $\dot{r}_{\min}$ (red dashed line, $r_{\min} = u_v$), the clear symmetry of the profiles around $r_{\min}$, and a self-similar shape (the rescaled profiles are well superimposed).

Between these two regimes, $\dot{r}_{\min}$ oscillates and reaches successively u_{iv} and u_v. While in Fig. 5*E*, the profiles do look like the self-similar profiles, they do not collapse satisfactorily (especially for positive values of ξ_1). Furthermore, the width of the error bars in Fig. 5*E* is comparable to the size of the data points and thus they cannot explain the differences between the three curves. In Fig. 5*D*, the situation is more obvious: The profiles are clearly not superimposed, and we even lose the symmetry of the profiles, even though this condition is essential for the calculation leading to Eq. **3**. It is clear that self-similarity is at least lost during the evolution of the neck close to breakup in Fig. 5*D*, whereas we can only speculate that it is also the case in Fig. 5*E*. Overall, these results suggest that self-similarity is lost during the oscillation of the neck radial velocity. After having identified the two self-similar regimes, we measure the duration of the transition between them. This duration increases dramatically both with the cylinder radii $R_{\rm cyl}$ and the velocity $v_{\rm cyl}$ as it can reach up to 50 ms (*SI Appendix*, Fig. S2), hiding somehow the self-similar features of the pinch-off for most of the process.

In conclusion, our results provide experimental proof of a log-oscillation of the slope of $r_{\min}$ in a viscous pinching process, during the transition from the viscous regime to the inertial–viscous one. In particular, this oscillating transition delays the onset of the final inertial–viscous regime. Moreover, an important consequence of this oscillation concerns the shape of the liquid filament which apparently does not follow any of the self-similar regimes along these transient dynamics, despite the values of $\dot{r}_{\min}$ alone suggesting otherwise. Contrary to many beliefs, the simple knowledge of $\dot{r}_{\min}$ during a linear regime is not sufficient to conclude that self-similarity is observed. Even though one would expect that external conditions play no role in this oscillatory behavior, we find that such a phenomenon appears when one end of the viscous filament is connected to either a large enough structure or a moving one (at a sufficient velocity). The influence of such quantities on the triggering of oscillations in the transient regime has yet to be investigated. Finally, it is surprising that the slopes for the minimum radius evolution in the oscillation are identical to those of the linear viscous and inertial–viscous regimes. The link between these dynamics and the lack of self-similar profiles in this region needs therefore to be clarified.

Materials and Methods

Oil Droplets. To perform the reference experiment of an oil droplet detaching from a needle of radius $R_{\rm needle}$, we extrude oil with a syringe pump (Harvard Apparatus PHD 2000) inside deionized water, at a very low flow rate Q = 0.1 mL/min, to form drops quasi-statically. As a consequence, the Weber number $We = \rho U^2 R_{needle}/\sigma$ verifies $We \ll 1$, with U the velocity of the fluid at the tip of the needle, so that the flow rate does not impact the dynamics. We use silicone oil (kinematic viscosity ν = 10^{-4} $m^2{\cdot}s^{-1}$, density ρ = 966 $kg{\cdot}m^{-3}$, oil–water interfacial tension γ = 42 $mN{\cdot}m^{-1}$). The needles used have a circular orifice of known inner and outer diameters. Because the oil wets the surface of the needle, the important dimension is only the outer diameter.

Stretched Meniscus Formed by a Moving Cylinder Pinned to the Oil–Water Interface. For the cylinder experiment, we fill a tank of dimensions 0.2 × 0.2 × 0.25 m with deionized water and add on top of it a 2-mm–thick layer of the same silicone oil as for the needle experiment. We pull on the interface with aluminum cylinders within a range of diameters from $2R_{\rm cyl}$ = 1 mm to 30 mm, with a Thorlabs Linear Translation Stage mounted with a stepped motor that can reach a velocity $v_{\rm cyl}$ = 30 mm/s along a travel range of 150 mm. To move the cylinder quasi-statically ($v_{\rm cyl}$ = 0), we control its vertical motion in 10-μm increments close to pinch-off and wait a few seconds between each step to leave enough time for the Plateau–Rayleigh instability to grow. If no thinning is observed, the cylinder is then moved downward again. This operation is repeated until thinning is triggered.

To ensure the reproducibility of our experiments, we check that the initial vertical position of the cylinder, when the motion is started, has no effect on the thinning dynamics. To that end, we reproduce several times the same experiment (with a given cylinder radius $R_{\rm cyl}$ and a given vertical velocity $v_{\rm cyl}$), but for different initial positions. The evolution of $r_{\min}$ is found to be the same in each experiment. Finally, for all experiments, we choose the initial acceleration profile (to increase the vertical velocity of the cylinder from 0 to $v_{\rm cyl}$) so that the constant velocity $v_{\rm cyl}$ is reached before the meniscus begins to thin.

Acquisition. A high-speed camera (Phantom v2511) records the dynamics with a recording speed up to 25,000 frames per second. To resolve perfectly the contour of the drop, we place between the backlight and the sample a mask, to increase the contrast with the ambient fluid.

Log-Oscillation. Without conducting the full calculation, we remind the reader how $\log(\tau)$ is the relevant measure of time to characterize the convergence toward a self-similar regime. For that purpose, we consider the equations leading to the inertial–viscous regime and follow the procedure developed by Eggers (18),

$$\rho(\partial_t v + v\partial_z v) = -\gamma\partial_z\left(\frac{1}{R_1}+\frac{1}{R_2}\right)+3\mu\frac{\partial_z(r^2\partial_z v)}{r^2}-\rho g \qquad [8]$$

$$\partial_t r + v\partial_z r = -r\partial_z v/2$$

with R_1 and R_2 the two radii of curvature, r the radius of the fluid filament, ρ its density, μ its viscosity, γ its surface tension, and v the velocity of the fluid. In the pinch region, r and v can be described with two self-similar functions ϕ and ψ and a single variable $z/\tau^{1/2}$, with τ the time remaining before pinch-off and z the vertical position. Such an approach leads to the asymptotic inertial–viscous regime, but if we want to capture the transition toward this regime, we need to keep a time dependency in ϕ and ψ, as in Eq. **9**,

$$r(z,t) = l_\mu \tau' \phi(z'/\tau'^{1/2},\tau') \qquad [9]$$
$$v(z,t) = (l_\mu/t_\mu)\tau'^{-1/2}\psi(z'/\tau'^{1/2},\tau')$$

with $\tau' = (t_{\rm po}-t)/t_\mu$ the dimensionless time before breakup and $z' = (z - z_{\rm po})/l_\mu$ the dimensionless vertical position. We define $\xi = z'/\tau'^{1/2}$ as the self-similar variable. Inserting Eq. **9** into Eq. **8** leads to a system of equations almost similar to the one obtained by Eggers, with only an additional term:

$$-\frac{\partial\psi}{\partial\log\tau'}+\frac{\psi}{2}+\xi\frac{\partial_\xi\psi}{2}+\psi\partial_\xi\psi=\frac{\partial_\xi\phi}{\phi^2}+3\partial_\xi^2\psi+6\frac{\partial_\xi\psi\partial_\xi\phi}{\phi}$$
$$-\frac{\partial\phi}{\partial\log\tau'}+\partial_\xi\phi\left(\psi+\frac{\xi}{2}\right)=\phi\left(1-\frac{\partial_\xi\psi}{2}\right). \qquad [10]$$

As we can see, the time τ' intervenes in the equations only through $\log(\tau')$ so that the dynamics around the self-similar solutions involve the log of the time only.

ACKNOWLEDGMENTS. We gratefully acknowledge Matthieu Roché for his useful comments at various stages of this work.

1. Ambravaneswaran B, Subramani HJ, Phillips SD, Basaran OA (2004) Dripping-jetting transitions in a dripping faucet. *Phys Rev Lett* 93:034501.
2. Sirringhaus H, et al. (2000) High-resolution inkjet printing of all-polymer transistor circuits. *Science* 290:2123–2126.
3. Xu T, Jin J, Gregory C, Hickman JJ, Boland T (2005) Inkjet printing of viable mammalian cells. *Biomaterials* 26:93–99.
4. Eggers J (1997) Nonlinear dynamics and breakup of free-surface flows. *Rev Mod Phys* 69:865–930.
5. Eggers J, Villermaux E (2008) Physics of liquid jets. *Rep Prog Phys* 71:036601.
6. Cohen I, Brenner MP, Eggers J, Nagel SR (1999) Two fluid drop snap-off problem: Experiments and theory. *Phys Rev Lett* 83:1147–1150.
7. Cohen I, Nagel SR (2001) Testing for scaling behavior dependence on geometrical and fluid parameters in the two fluid drop snap-off problem. *Phys Fluids* 13:3533–3541.
8. Zhang WW, Lister JR (1999) Similarity solutions for capillary pinch-off in fluids of differing viscosity. *Phys Rev Lett* 83:1151–1154.
9. Sierou A, Lister JR (2003) Self-similar solutions for viscous capillary pinch-off. *J Fluid Mech* 497:381–403.

10. Shi X, Brenner MP, Nagel SR (1994) A cascade of structure in a drop falling from a faucet. *Science* 265:219–222.
11. Doshi P, et al. (2003) Persistence of memory in drop breakup: The breakdown of universality. *Science* 302:1185–1188.
12. Schmidt LE, Keim NC, Zhang WW, Nagel SR (2009) Memory-encoding vibrations in a disconnecting air bubble. *Nat Phys* 5:343–346.
13. Castrejón-Pita JR, et al. (2015) Plethora of transitions during breakup of liquid filaments. *Proc Natl Acad Sci USA* 112:4582–4587.
14. Li Y, Sprittles JE (2016) Capillary breakup of a liquid bridge: Identifying regimes and transitions. *J Fluid Mech* 797:29–59.
15. Rayleigh L (1879) On the capillary phenomena of jets. *Proc R Soc Lond* 29: 71–97.
16. Rayleigh L (1892) Xvi. On the instability of a cylinder of viscous liquid under capillary force. *London Edinburgh Dublin Philos Mag J Sci* 34:145–154.
17. Papageorgiou DT (1995) On the breakup of viscous liquid threads. *Phys Fluids* 7:1529–1544.
18. Eggers J (1993) Universal pinching of 3D axisymmetric free-surface flow. *Phys Rev Lett* 71:3458–3460.
19. Rothert A, Richter R, Rehberg I (2003) Formation of a drop: Viscosity dependence of three flow regimes. *New J Phys* 5:59.
20. Rothert A, Richter R, Rehberg I (2001) Transition from symmetric to asymmetric scaling function before drop pinch-off. *Phys Rev Lett* 87:084501.
21. Lister JR, Stone HA (1998) Capillary breakup of a viscous thread surrounded by another viscous fluid. *Phys Fluids* 10:2758–2764.